

Article

Hydro-Mechanical Coupling Analysis of Field Pumping Test in Granite Residual Soil Site

Zefu Li, Yadong Li *, Shuyu Nie, Zikang Pang, Jie Cui and Yi Shan * 

School of Civil Engineering and Transportation, Guangzhou University, Guangzhou 511370, China; 2112316010@e.gzhu.edu.cn (Z.L.); gzdwnieshuyu@163.com (S.N.); 2112416134@e.gzhu.edu.cn (Z.P.); jcui2009@hotmail.com (J.C.)

* Correspondence: liyadong@gzhu.edu.cn (Y.L.); yshan@gzhu.edu.cn (Y.S.)

Abstract

In addressing the challenge that the settlement behavior of granite residual soil in South China during foundation pit dewatering cannot be fully understood due to its unsaturated characteristics, this study proposes and validates an unsaturated fluid–solid coupling calculation method for dewatering-induced settlement analysis. This method is implemented by compiling FISH language code within a finite difference software framework. Validation was carried out by comparing the simulated groundwater drawdown–time response with the measured drawdown from a field pumping test, demonstrating the improved agreement of the proposed unsaturated coupling approach relative to the conventional coupling scheme. Furthermore, to elucidate the soil settlement mechanisms, a sensitivity analysis of the deformation behavior of granite residual soil during dewatering was performed. The results demonstrate that, compared to the traditional fluid–solid coupling method, the unsaturated fluid–solid coupling method exhibits superior agreement with field dewatering experiments. The sensitivity analysis reveals that the differential settlement observed in the soil surrounding a dewatering well under the same target drawdown is primarily attributed to variations in drainage consolidation time and pore water pressure dissipation. Finally, a normalized analysis correlating the dewatering depth at the well with the resulting soil settlement deformation was conducted, establishing a practical relationship applicable under similar ground conditions and dewatering durations. This analysis provides theoretical guidance for selecting appropriate dewatering schemes during engineering practice.

Keywords: unsaturated; fluid–structure coupling; granite residual soil; pumping test; sedimentation



Academic Editor: Eugeniusz Koda

Received: 28 January 2026

Revised: 24 February 2026

Accepted: 1 March 2026

Published: 3 March 2026

Copyright: © 2026 by the authors.

Licensee MDPI, Basel, Switzerland.

This article is an open access article distributed under the terms and conditions of the [Creative Commons Attribution \(CC BY\)](https://creativecommons.org/licenses/by/4.0/) license.

1. Introduction

With the rapid advancement of urbanization in China, urban functions are evolving toward high density and mixed use, while developable surface space is becoming increasingly saturated. Consequently, development priorities are gradually shifting to underground space, and the number and scale of underground facilities continue to expand. Engineering projects such as metro stations and running tunnels, underground utility tunnels, and underground commercial and municipal facilities have proliferated, leading to a substantial increase in both the proportion and complexity of deep foundation pit engineering in urban construction systems. In underground construction, foundation pit excavation and dewatering constitute critical procedures. During foundation pit dewatering, the redistribution and dissipation of pore water pressure in the soil, together with the formation of a cone

of depression, can readily induce uneven ground settlement around the foundation pit, thereby threatening the safety of adjacent buildings [1,2]. Field monitoring and coupled analyses indicate that groundwater drawdown induced by foundation pit dewatering is accompanied by a reduction in pore water pressure and consolidation compression of the soil, which in turn generates large-area ground/building settlement around the foundation pit, with part of the settlement being evidently irreversible [3,4]. Meanwhile, under conditions of hydraulic connectivity or imperfect cut-off, pumping within the pit may interact with deformation of the retaining structure and further aggravate settlement outside the pit, potentially triggering damage risks to nearby existing buildings [4,5].

Granite residual soil, a regional soil widely distributed in South China, is strongly affected by intense weathering, leaching, and reworking. In its natural state, it generally exhibits certain bearing capacity and constructability and is therefore widely used as a major foundation bearing stratum for buildings and structures, as well as metro tunnels, in the Guangdong–Hong Kong–Macao Greater Bay Area. However, this soil shows pronounced water sensitivity and structural features; once immersed, it is prone to rapid softening and disintegration, which may subsequently lead to a reduction in foundation bearing capacity [6] and cause engineering accidents such as cracking of the superstructure. Weathered granite soil under dewatering-induced seepage may undergo not only consolidation and evolution of unsaturated behavior but also suffosion triggered by fine-particle migration, which can accelerate pore-structure deterioration and amplify the settlement response [7,8]. To meet the needs of safe urban underground construction and environmental protection, it is essential to understand, before and during construction, the deformation evolution and deterioration of mechanical performance of granite residual soil under hydraulic actions, so as to provide reliable support for the optimization of foundation pit dewatering schemes, settlement prediction, and risk prevention and control. Accordingly, extensive studies have been conducted by researchers worldwide.

Li et al. [9], based on field evidence of additional deformation of an existing shield tunnel induced by deep foundation pit dewatering in soft soil strata with leaky aquifers, indicated that the groundwater drawdown caused by dewatering may result in tunnel settlement and that targeted control measures are required. Li et al. [10] collected field data from ten pumping tests conducted in Shanghai, performed statistical analyses on dewatering depth and ground settlement, and established a coupled hydro-mechanical model based on Biot's three-dimensional consolidation theory with an explicit solution scheme, revealing that the compressibility of each soil layer is closely associated with the decline in pore pressure. Wen D. et al. [11] investigated a large number of foundation pit excavation projects in Singapore and found that, when granite residual soil exhibits high permeability and the underlying rock mass is highly fractured, foundation pit dewatering may cause a substantial decline in the surrounding groundwater level and thus induce settlement. Thomas et al. [12], based on unsaturated soil theory, proposed a finite-element–finite-difference numerical method for unsaturated clay to simulate the evolution of degree of saturation during thermally induced drying, and validated the numerical results against field measurements, demonstrating that the proposed method can accurately capture the saturation response of unsaturated clay under thermal drying. Chu et al. [13], taking a foundation pit in the soft-soil area of Zhuhai as an example, investigated a common dewatering system consisting of a “suspended cut-off curtain + pumping wells”. By combining the equivalent-well concept with MODFLOW numerical analysis, they developed a prediction method for in-pit drawdown and quantified the effects of key parameters such as curtain embedment depth and screen length on drawdown control, thereby providing quantitative guidance for dewatering design. Wang et al. [14] conducted field pumping–recharge tests at a super-large deep foundation pit group site in Shang-

hai, showing that recharge can raise the groundwater level and reduce settlement; they further recommended identifying aquifer connectivity through pumping–recharge tests prior to construction to guide the dewatering–recharge scheme. Zhu et al. [15], based on three-dimensional hydro-mechanical coupled analysis, further suggested that controlling the pumping rate and improving the water cut-off performance of TRD cut-off walls can reduce dewatering-induced retaining-structure deformation and environmental settlement. In addition, Pujades et al. [16] compared the effectiveness of “deepening the enclosure” versus “pumping dewatering” in reducing settlement outside the pit, and pointed out that simply deepening the enclosure has limited capability to weaken the influence of external pumping; therefore, refined control of the pumping process is still required in engineering practice to mitigate settlement risks. Zhang et al. [17], based on field tests of deep foundation pits in Shanghai, proposed an integrated technique of “in-pit pumping + multi-well recharge near protected targets” to suppress drawdown and control settlement. Sun et al. [18] further adopted a “finite element–linear programming” simulation–optimization approach to optimize the combination of pumping wells, pumping sequence, and the upper limit of pumping rate for each well, achieving simultaneous reductions in drawdown and ground settlement.

However, during foundation pit dewatering, as the groundwater level declines, granite residual soil may transition from a saturated state to an unsaturated state, and its mechanical properties, hydraulic characteristics, pore water pressure, and permeability will change accordingly. The evolution of saturation and matric suction in the unsaturated zone alters relative permeability and pore-pressure diffusion, thereby modifying the effective-stress path and volumetric strain accumulation. Accordingly, explicitly accounting for unsaturated hydro-mechanical (HM) coupling is essential for analyzing dewatering-induced settlement. Recent numerical studies on unsaturated HM coupling commonly adopt a unified framework combining the soil–water characteristic curve/relationship (SWCC/SWRC; suction–saturation relationship), a relative-permeability function, and a soil-skeleton constitutive model, and update state variables such as suction and saturation via user subroutines to capture the influence of unsaturated evolution on pore-pressure fields and deformation responses [19,20]. However, for foundation-pit dewatering and groundwater drawdown, many existing seepage–stress coupling analyses still simplify the region above the groundwater table as either fully saturated or with zero pore pressure, thereby neglecting the saturation-driven evolution of permeability and compressibility in the unsaturated zone and potentially biasing the predicted late-stage drawdown and settlement time histories. Meanwhile, within the Itasca ecosystem, secondary development has been used to enhance FLAC3D’s capability for modeling unsaturated seepage processes and to support response analyses under rapid-drawdown conditions [21]. Building on this, this study conducts secondary development within the FLAC3D coupling framework using FISH to enable online updating of key unsaturated state variables and hydro-mechanical coupling parameters; because FISH can be invoked during the solution cycling to control parameters and variables, it provides direct support for establishing a reproducible unsaturated seepage–stress coupling workflow. The proposed method is validated against a field pumping test, and the coupled hydro-mechanical behavior under unsaturated conditions is effectively characterized. On this basis, the method is applied to investigate the settlement and deformation behavior of granite residual soil in the unsaturated state, providing a theoretical reference for engineering design under similar geological conditions.

2. Implementation of an Unsaturated Fluid–Structure Coupling Scheme in FLAC3D Using FISH

2.1. Coupling Strategy for Unsaturated Fluid–Structure Coupling

In conventional seepage analysis, FLAC3D assumes that the pore water pressure above the groundwater table is zero, whereas the degree of saturation below the groundwater table is forcibly set to 1.0 at all times. Consequently, during computation the permeability in the unsaturated zone is still taken as the saturated permeability, which is inconsistent with unsaturated seepage theory. Meanwhile, the degree of saturation also affects soil density. Porosity is defined as the ratio of pore volume to the total soil volume. When soil compressibility is considered, compression of the soil mass reduces the pore volume and thus alters porosity; however, FLAC3D does not update porosity during calculation. This may amplify the computed change in fluid volume in seepage analysis and further compromise the accuracy of numerical results [7–10]. Therefore, based on the conventional fluid–structure coupling solver in FLAC3D, this study modifies the underlying coupling procedure using the platform-provided FISH language so that relevant calculation parameters can be updated in real time, thereby enabling simulation of unsaturated fluid–structure coupling. The unsaturated representation adopted in this study follows the standard framework of SWCC/SWRC (suction–saturation relation) + relative-permeability function + soil-skeleton constitutive model. The key contribution is to embed saturation-driven updates of hydraulic and coupling parameters into the FLAC3D hydro-mechanical iteration, establishing a reproducible online-updating workflow and benchmarking it against conventional simplifications (zero pore pressure or fully saturated conditions above the groundwater table) to elucidate how unsaturated evolution governs late-stage draw-down and settlement time histories.

To improve implementability and match the field pumping test, the model adopts several necessary simplifications: each stratum is represented by equivalent homogeneous parameters; layer interfaces are idealized as planar; the overburden is applied as equivalent stress; and the pumping well is represented by an axial drainage boundary rather than explicit well geometry. These simplifications control model complexity and reduce non-essential boundary/mesh effects; their implications are discussed in “Limitations”. Among the fully coupled options in FLAC3D (manual, master–slave, and direct-solution), the master–slave strategy is adopted because it enables stepwise transient coupling and allows FISH-based on-the-fly updating of key unsaturated parameters after each coupling cycle. Direct solution is not used because it is more sensitive to time-step/convergence control and is less convenient for embedding parameter-updating procedures.

In FLAC3D, three approaches are available for fully coupled analysis: the manual approach, the master–slave approach, and the direct solution approach. In this study, the master–slave approach, which is suitable for transient analysis, is adopted. In the master–slave approach, the seepage process serves as the master process and the mechanical process as the slave process. For each time step advanced by the master process, the corresponding data are transferred to the slave process. The slave process then performs a reasonable number of steps until equilibrium is achieved, after which the updated data are passed back to the master process. This loop continues until the end of computation. Moreover, by correcting parameters such as permeability, porosity, and soil density after equilibrium is reached in both seepage and mechanical calculations at each coupling cycle, engineering dewatering under unsaturated soil conditions can be simulated. The computational workflow is shown in Figure 1.

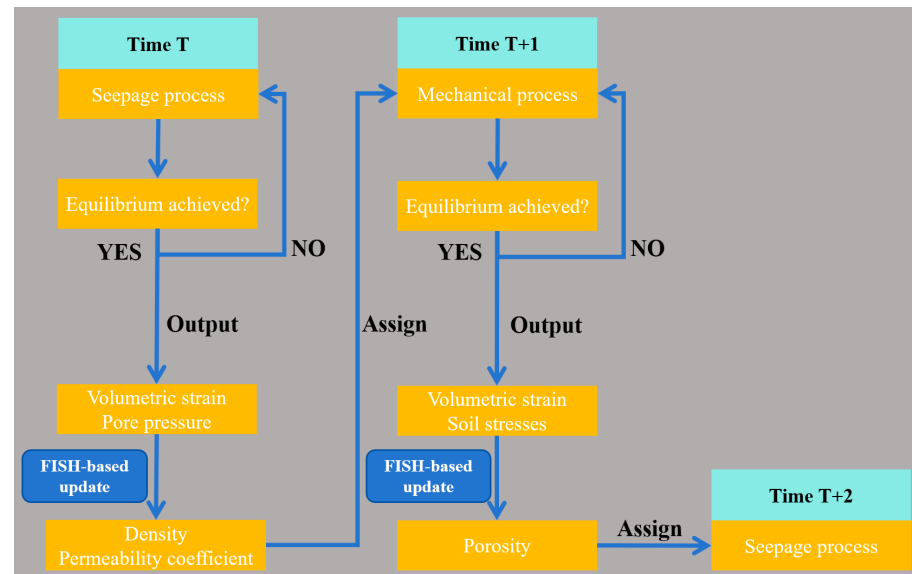


Figure 1. Workflow of unsaturated fluid–structure coupling.

To ensure continuous execution of the entire calculation, the WHILESTEPPING command provided by FLAC3D is required. This command executes the specified instruction after each calculation step. However, WHILESTEPPING itself cannot determine whether equilibrium has been achieved; therefore, parameter correction after each step can only be properly implemented when combined with an equilibrium criterion.

2.2. On-the-Fly Updating and Dynamic Correction of Coupling Parameters Using FISH

The FISH language in FLAC3D provides the FISHCALL command, which enables correction of seepage and mechanical parameters based on the computed results at each step. In seepage calculation, the relationship among fluid pore pressure, degree of saturation, and the change in fluid volume is expressed as Equation (1):

$$\frac{1}{M} \frac{dp}{dt} + \frac{ns}{s} \frac{d\zeta}{dt} = \frac{1}{s} \frac{d\zeta}{dt} \quad (1)$$

where M is the Biot modulus, which accounts for the compressibility of the soil skeleton and the pore water, and directly controls the dissipation rate of pore water pressure and the time-dependent effect of soil deformation during consolidation. In this study, M is estimated indirectly from the soil compression modulus and Poisson's ratio. n is porosity; t is time; and ζ denotes the change in fluid volume per unit volume of porous medium induced by diffusion. When the fluid is incompressible, ζ equals the change in element flow rate.

For saturated seepage analysis, FLAC3D sets the degree of saturation to 1.0 by default. Accordingly, the nodal pore water pressure at the next time increment is updated as Equation (2):

$$\frac{1}{M} \frac{dp}{dt} = \frac{1}{s} \frac{d\zeta}{dt} \quad (2)$$

After geostress equilibrium, the total volume of each zone is stored using the TABLE command in FISH. Once the seepage process reaches equilibrium, the fluid volume change in each zone is retrieved via FISH, allowing the true degree of saturation to be computed. With the true degree of saturation obtained, the permeability is corrected using the VGM

formulation, and the updated permeability is then assigned to all zones through traversal. The VGM equations are Equations (3) and (4):

$$k_{rl} = (s_e)^{0.5} \left[1 - \left(1 - (s_e)^{1/m} \right)^m \right]^2 \quad (3)$$

$$k_{rg} = (1 - s_e)^{0.5} \left[1 - \left(1 - s_e^{1/m} \right)^m \right]^2 \quad (4)$$

where k_{rl} is the liquid-phase permeability coefficient, s_e is the effective liquid saturation, and k_{rg} is the gas-phase permeability coefficient.

For mechanical calculation, once the mechanical process reaches equilibrium, the fluid volume change in each zone is read using FISH. Combined with the initially stored total zone volume, the true porosity can be computed and then updated for all zones. Porosity is defined as Equation (5):

$$n = \frac{V_v}{V} \quad (5)$$

2.3. Determination of Unsaturated Soil Parameters

The soil–water characteristic curve plays a critical role in the permeability behavior of unsaturated soils because it directly determines the distribution of permeability. The liquid-phase permeability coefficient k_{rl} and gas-phase permeability coefficient k_{rg} are quantitatively linked to the SWCC through the VGM formulation. When the soil exhibits a high degree of saturation, the SWCC shows a relatively gentle slope; k_{rl} approaches the saturated permeability, while k_{rg} is close to zero, indicating that seepage is dominated by the water phase. As pumping proceeds, the degree of saturation gradually decreases and matric suction increases; the SWCC slope becomes steeper, k_{rl} decays nonlinearly according to the VGM formulation, and k_{rg} increases progressively, such that seepage transitions from single-phase water flow to two-phase water–gas flow. When the degree of saturation decreases to the residual water content, k_{rl} tends to a stable minimum and k_{rg} reaches its maximum, implying that seepage is dominated by the gas phase. This linkage ensures that, in unsaturated fluid–structure coupling simulations, the dynamic update of permeability with degree of saturation is consistent with realistic seepage behavior.

To accurately characterize the soil–water characteristic curve of granite residual soil, this study fits the experimental results reported by Fung [22]. Fung obtained the soil–water characteristic curve data of completely weathered granite residual soil through laboratory tests and proposed an appropriate fitting model. Because granite residual soil exhibits distinct SWCC behaviors over different ranges of matric suction, piecewise fitting is necessary. In the low-suction range (matric suction < 2.4 kPa), the water content decreases rapidly and the curve is steep; in the high-suction range (matric suction \geq 2.4 kPa), the decrease in water content becomes gradual and the curve flattens. Piecewise fitting better captures the water-retention characteristics across different suction ranges and avoids the insufficient accuracy that may arise when a single model is forced to fit the full suction range, thereby providing a closer representation of the actual water-retention behavior of granite residual soil. The fitting parameters ($a = 0.293771$, $m = 1.841928$, $n = 0.270943$) have been verified in relevant studies on unsaturated granite residual soil and can accurately describe the relationship between matric suction and water content. Accordingly, the unsaturated soil parameters in this study adopt those reported by Fung. The SWCC parameters are adopted mainly because the tested material (completely weathered granite residual soil) is comparable to the engineering soil considered in this study in terms of soil type and regional context, and the same parameter set has been repeatedly used in related studies. It should be noted that directly transferring the SWCC parameters may affect saturation evolution and the associated permeability–pore-pressure diffusion process,

and thus the late-stage drawdown and settlement time histories; therefore, the applicability bounds and implications for result interpretation are stated in “Limitations”. A piecewise function is used to fit Fung’s soil–water characteristic curve test results (Figure 2) [23], as expressed by:

$$\begin{cases} \theta = \theta_s & x < 2.4 \\ \theta = \frac{\theta_s}{\ln\left(e + \left(\frac{\psi}{a}\right)^n\right)^m} & x \geq 2.4 \end{cases} \quad (6)$$

where θ is the volumetric water content, θ_s is the saturated volumetric water content, ψ is matric suction, and a , m , and n are model parameters. In this study, $a = 0.293771$, $m = 1.841928$, and $n = 0.270943$.

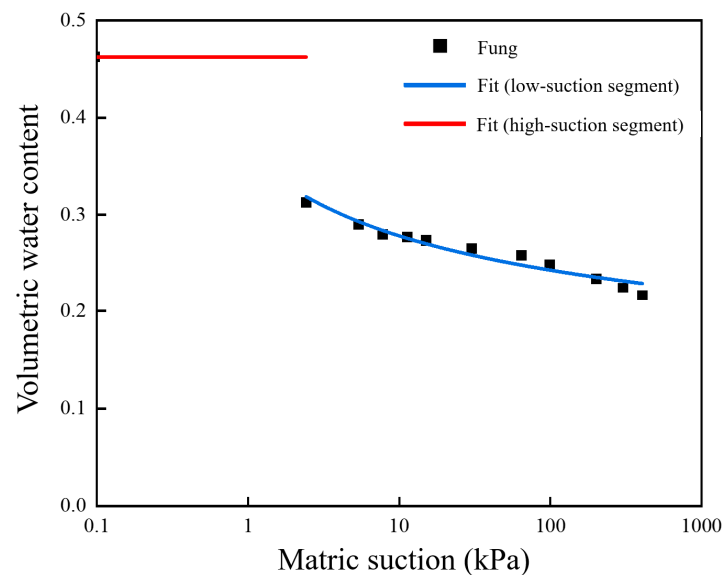


Figure 2. Soil–water characteristic curve.

3. Verification of the Proposed Unsaturated Fluid–Structure Coupling Method

To verify the reliability of the proposed unsaturated fluid–structure coupling method, a field pumping test was conducted and a three-dimensional numerical model was developed. By comparing field measurements with numerical results, the applicability of the proposed method was assessed. The pumping test was carried out at a project site in Huangpu District, Guangzhou, with granite residual soil as the target stratum. Key hydrogeological parameters (e.g., hydraulic conductivity, radius of influence, and discharge of a single well) were determined through the field pumping test. Meanwhile, groundwater-level variation was monitored to support model validation; ground-settlement monitoring was also implemented, but the data were insufficient for a rigorous quantitative validation due to the short test duration and the low permeability of the stratum.

3.1. Field Pumping Test

(1) Project Overview

According to the detailed geotechnical investigation report, the conventional soil parameters of each layer are summarized in Table 1. The initial groundwater level observed in boreholes was 3.00–3.50 m below ground surface, while the stable groundwater level was 3.20–3.50 m. The aquifer thickness was 16 m. Three pumping scenarios were designed, where the maximum target drawdown of 14 m was defined as 100% drawdown, and the other two scenarios were set as 75% and 40% drawdown relative to this target. The

drawdown was controlled by adjusting the pumping discharge, and each subsequent pumping scenario was conducted only after the groundwater level had recovered to a stable condition.

Table 1. Conventional soil parameters for each layer.

Soil Type	Density (kg/m ³)	Layer Depth (m)	Deformation Modulus (MPa)	Cohesion (kPa)	Internal Friction Angle (°)
Mixed Soil	1600	6.20	5	8	13
Fine Clay	1900	7.10	15	23	13
Medium Sand	1950	8.40	22	2	27
Sandy Plastic Soil	1850	11.00	20	24	19
Flower Rock Residue Soil	1850	16.90	30	26	20
Fully Weathered Flower Rock	1900	32.90	75	28	22

The pumping well was constructed using a drilling rig with a borehole diameter of 168 mm. A ϕ 110 mm stainless-steel casing was installed, and high-quality clay balls were used to seal the annular space outside the casing to ensure adequate sealing. The well configuration is illustrated in Figure 3.

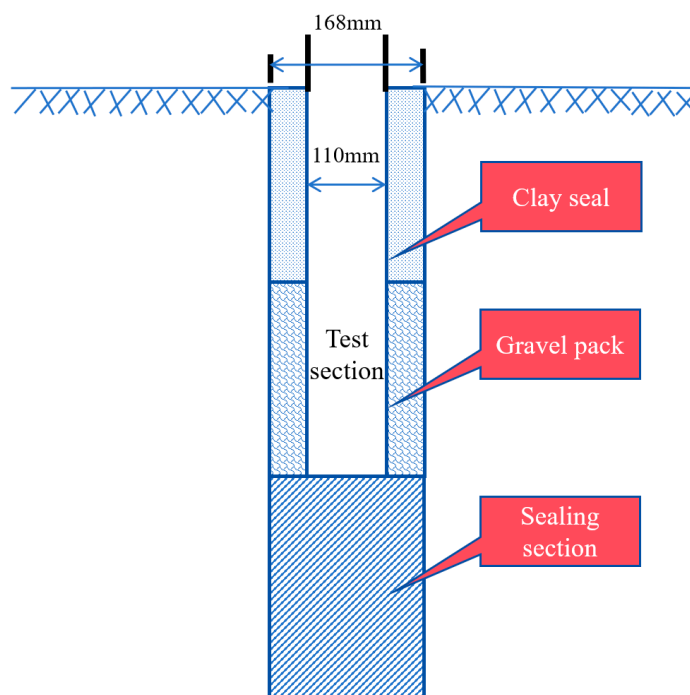


Figure 3. Well casing configuration.

(2) Results and Response Characteristics of the Pumping Test

After completion of the pumping test, the hydraulic conductivity, radius of influence, and other parameters of a confined aquifer fully penetrating well were calculated using the corresponding equations [23]. The time histories of groundwater drawdown under different scenarios are shown in Figure 4. During the first 20 min of pumping, the groundwater level in the pumping well dropped rapidly, reaching approximately 90% of the target drawdown at 20 min. After about 1 h, the groundwater level essentially reached the target drawdown and became stable.

As summarized in Table 2, the maximum measured drawdown was 14.21 m, and the maximum discharge was 10.648 m³/d. The hydraulic conductivity derived from this pumping test was 0.076 m/d, indicating a low-permeability soil, and the maximum radius of influence was 39.17 m.

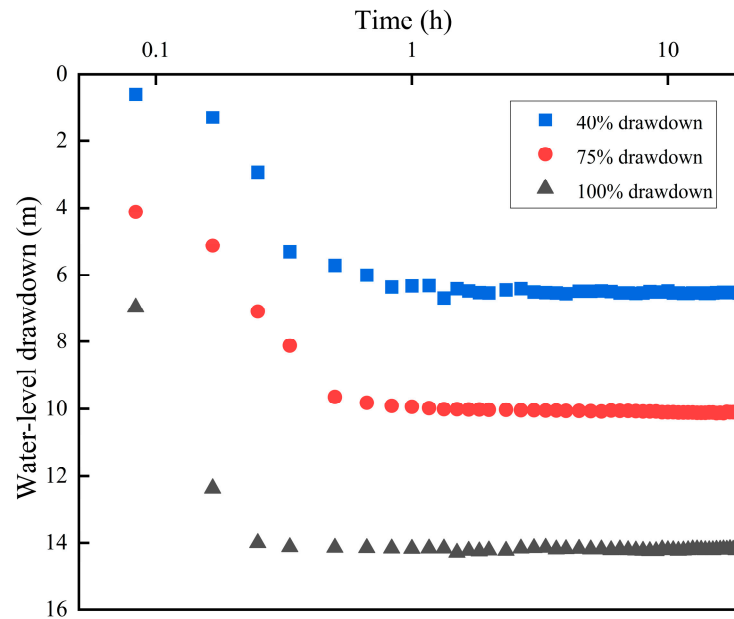


Figure 4. Groundwater drawdown curve.

Table 2. Analysis of pumping test equipment and results.

Test Type	Aquifer Thickness (m)	Well Diameter (m)	Pumping Time (h)	Actual Drawdown (m)	Pumping Rate (m ³ /d)	Permeability Coefficient (/m/d)	Influence Radius (m)
100% Drawdown	16	0.055	24	14.21	10.648	0.076	39.17
75% Drawdown	16	0.055	24	10.12	7.982	0.078	22.56

3.2. Development of the 3D Numerical Model in FLAC3D

To capture the coupled evolution of the dewatering process in both the plan view and the vertical direction, the computational domain is defined as a three-dimensional spatial domain $\Omega \subset R^3$. The primary unknowns in Ω include the displacement vector $u(x, y, z, t)$, the pore-water pressure $u_w(x, y, z, t)$, and the degree of saturation $S_r(x, y, z, t)$. The pore-pressure variation and the expansion of the unsaturated zone induced by dewatering are described by an unsaturated seepage (flow) equation and are coupled with the mechanical equilibrium of the soil skeleton, thereby enabling the three-dimensional distribution of settlement responses to be obtained. From an engineering idealization perspective, a two-dimensional plane-strain model usually implies that the geometry and loading/dewatering conditions are approximately uniform along the longitudinal direction of the foundation pit, whereas a one-dimensional model further assumes lateral uniformity with vertically layered soil being dominant. Therefore, the choice of model dimensionality essentially depends on whether these idealized assumptions are acceptable for the engineering problem. In this study, a three-dimensional formulation is adopted to maintain consistency between the problem definition and practical conditions when plan-view non-uniformities exist, and to provide a more coherent spatial representation of the unsaturated coupling mechanism.

The purpose of adopting a three-dimensional model is not to pursue additional complexity, but to preserve the spatial variability in the “drawdown cone–deformation response” under well dewatering conditions. In contrast, two-dimensional plane-strain and one-dimensional models typically rely on idealized assumptions of approximate uniformity in geometry and boundary conditions along one direction, and their applicability depends on whether the field conditions satisfy such prerequisites. Previous studies on deep excavations have shown that corner effects, boundary distances, and in-plane non-

uniformities may induce pronounced three-dimensional effects; under these circumstances, plane-strain simplification may partially smooth out or underestimate the spatially varying response and should therefore be used with caution within its applicability range [24–26]. In addition, practical dewatering problems may exhibit in-plane hydraulic gradients due to factors such as cut-off wall leakage or flow diversion caused by obstacles (e.g., existing pile groups), for which a three-dimensional hydro-mechanical coupling framework provides a more consistent description of the linkage between drawdown and deformation [27,28]. The mechanistic interpretation and parameterization of unsaturated effects in this study are built upon well-established theoretical frameworks, including the VG–Mualem relationships and classical extensions of effective stress concepts for unsaturated soils [29,30].

The overlying strata above the test layer are dominated by clay and can be regarded as weakly permeable. To simplify the calculation procedure, improve computational efficiency, and optimize seepage interactions among layers, the water body within the test-layer drawdown range was idealized as a confined-aquifer model. The mechanical behavior of the soil was assumed to follow the Mohr–Coulomb criterion, and the seepage behavior was assumed to obey Darcy’s law. Prior to pumping, the soil was assumed to be normally consolidated. After pumping commenced, the unsaturated characteristics of the confined-aquifer soil were considered to investigate its deformation during unsaturated seepage. Given the model idealizations, a sector domain representing the test layer from 16.90 to 32.90 m was selected as the primary simulation domain. The main Mohr–Coulomb parameters used in the numerical model are listed in Table 3. The interfaces of all soil layers were assumed to be planar, neglecting local thickness undulations. The overburden from 0 to 16.90 m was represented by applying equivalent stresses according to the modeling assumptions. A graded mesh was adopted. To further simplify the model and reduce computational time, the physical structure of the pumping well was not explicitly modeled. Instead, a drainage boundary condition was imposed along the axis to represent the dewatering effect of the pumping well. The 3D numerical model is shown in Figure 5.

Table 3. Model parameters for fully weathered flower rock.

Parameter	Fully Weathered Flower Rock
Density (kg/m ³)	1900
Poisson’s Ratio	0.53
Porosity	0.42
Deformation Modulus (MPa)	75
Compressive Modulus (MPa)	30
Cohesion (kPa)	28
Internal Friction Angle (°)	31
Permeability Coefficient (m/d)	0.076

Based on the pumping-test results, the maximum radius of influence was 39.17 m. To mitigate boundary effects on numerical results, the horizontal model size was set to 100 m [31]. Moreover, to represent seepage toward a fully penetrating well in a confined aquifer, the drainage boundary was implemented using a nodal/zone flux assignment scheme, i.e., prescribing the inflow/outflow discharge rate at nodes or zones.

The numerical simulation followed these steps:

1. Step 1 (Geostatic equilibrium): establish the initial stress state based on burial depth, effective unit weight, and the at-rest earth pressure coefficient; initialize the pore water pressure field; and apply boundary conditions.
2. Step 2 (Equilibrium check and displacement reset): verify the geostatic equilibrium and reset displacements to avoid interference with subsequent calculations.
3. Step 3 (Pumping simulation): apply the pumping boundary, activate the unsaturated fluid–structure coupling code, simulate the field pumping test, and monitor

groundwater drawdown, ground settlement, and degree of saturation; finally, output the results.

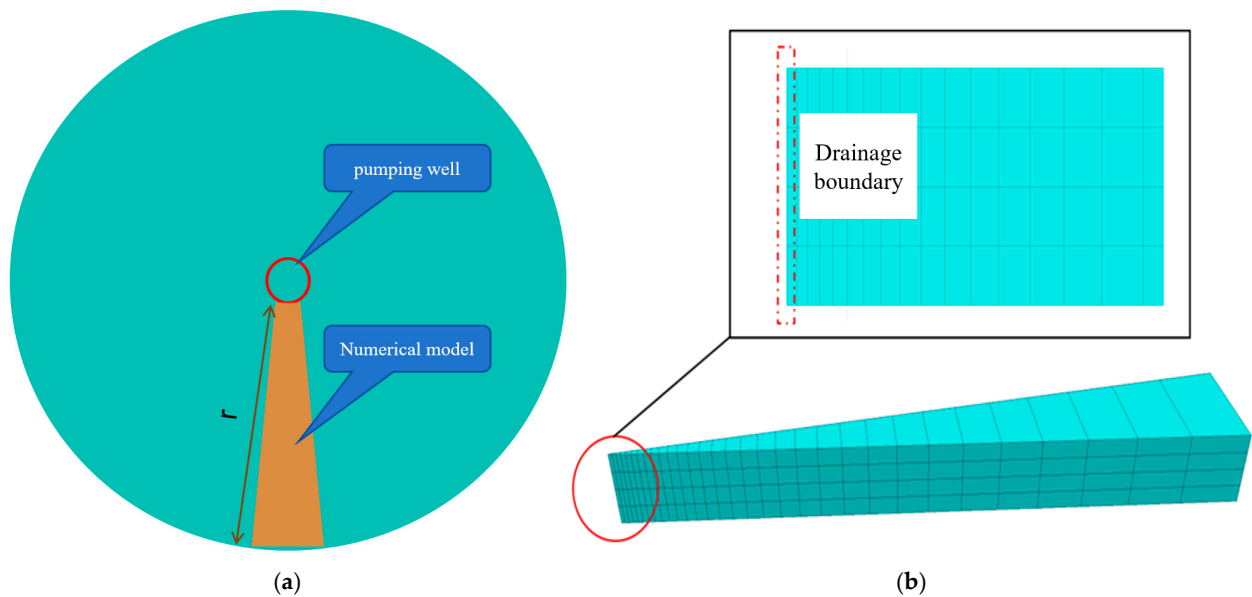


Figure 5. 3D numerical model: (a) Simplified model; (b) Drainage boundary layout.

3.3. Model Validation and Discussion

Model verification in this study is primarily based on reproducing the time history and stabilized value of groundwater drawdown observed in the field pumping test; therefore, the settlement results are used to compare the numerical differences between the conventional and unsaturated coupling schemes under the same pumping boundary condition, rather than to fit or evaluate errors against field settlement data. To improve clarity, Section 3.3 is organized around (i) drawdown behavior, (ii) settlement response, and (iii) saturation evolution and its implications.

(1) Groundwater Drawdown

After geostatic equilibrium of the unsaturated fluid–structure coupling model, the initial stress state was checked. The pore water pressure contours for the initial state and the 100% drawdown scenario are shown in Figure 6a. In the initial state, pore water pressure was uniform over the entire domain with no hydraulic gradient, remaining stable at 174 kPa, corresponding to a groundwater level of approximately 3.2–3.5 m. Under the 100% drawdown scenario, pore water pressure dissipated and effective stress increased, forming a funnel-shaped distribution centered at the pumping well. The pore water pressure in the core region decreased markedly, consistent with the theoretical behavior of seepage toward a fully penetrating well in a confined aquifer. In the 3D model, the drainage boundary was implemented by prescribing a seepage flux/velocity, and thus groundwater drawdown is one of the model outputs. Model accuracy was evaluated by comparing the computed drawdown with field measurements.

The drawdown curves at 60 min are shown in Figure 6b. Field measurements indicate that in the 0–10 min stage, the drawdown curve is approximately linear, implying an approximately constant pumping rate; by 20 min, the measured drawdown tends to stabilize. In contrast, the computed drawdown shows a higher drawdown rate during 0–5 min, followed by an abrupt reduction in slope during 5–10 min, i.e., the drawdown rate becomes much smaller than the measured one. After 10 min, the computed slope gradually decreases and the drawdown approaches a stable value.

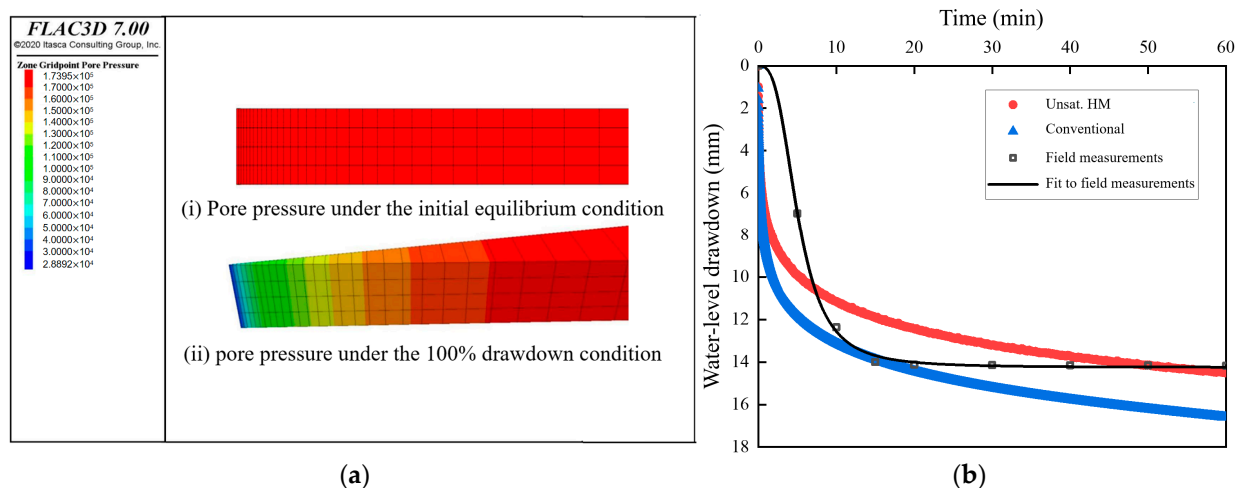


Figure 6. Comparison between simulation results and field measurements: (a) Simulation results; (b) Water level drawdown.

Although identical pumping boundary conditions were adopted in both numerical models, the drawdown curve of the unsaturated fluid–structure coupling model exhibits a smaller slope than that of the conventional fluid–structure coupling model, and the discrepancy increases with pumping duration. Regarding the final stabilized drawdown, the unsaturated fluid–structure coupling result is closer to the field measurement, indicating higher accuracy. This is because in the unsaturated fluid–structure coupling model, drawdown reduces the degree of saturation in the aquifer, which in turn decreases permeability. Consequently, the seepage flux through a given cross-section decreases progressively with time, and the drawdown-rate difference between the two models increases. Therefore, for engineering dewatering simulations in confined aquifers, the unsaturated fluid–structure coupling model provides a more realistic representation and improved accuracy compared with the conventional fluid–structure coupling model.

(2) Ground Settlement

Due to project constraints, the duration of the field pumping test was relatively short, and the permeability of the test stratum was low. As a result, the ground-settlement monitoring points did not yield effective field data. Therefore, this section focuses on comparing the computed ground settlement from the two numerical models.

The ground-settlement contours after 60 min of pumping are shown in Figure 7a. The maximum settlement occurs at the pumping well, with a peak value of 4.33 mm. Based on the maximum radius of influence of 39.17 m obtained from the pumping test, the settlement decreases with increasing distance from the well, and the settlement influence tends to stabilize beyond approximately 30 m, which is close to the pumping-test-derived radius of influence. The conventional fluid–structure coupling model produces lower settlement values, which may cause engineers to underestimate the environmental impact of engineering dewatering and thereby increase the risk of adverse engineering incidents [32–34].

(3) Evolution of Degree of Saturation

The degree of saturation provides an intuitive indicator of pore-water content within the soil. The distributions of degree of saturation in the aquifer at different pumping times are shown in Figure 7b. The results indicate that the degree of saturation decreases most rapidly within 0–5 m around the pumping well, and the rate of decrease diminishes with distance. For equal time intervals, the difference between curves becomes smaller, implying that the rate of decrease in degree of saturation gradually reduces with time, i.e., the drawdown rate gradually decreases. This behavior is consistent with the field observation

that discharge decreases with pumping duration. The numerical model developed in Section 3.3 clearly captures the progressive reduction in degree of saturation induced by pumping and enables visualization of saturation changes during engineering dewatering.

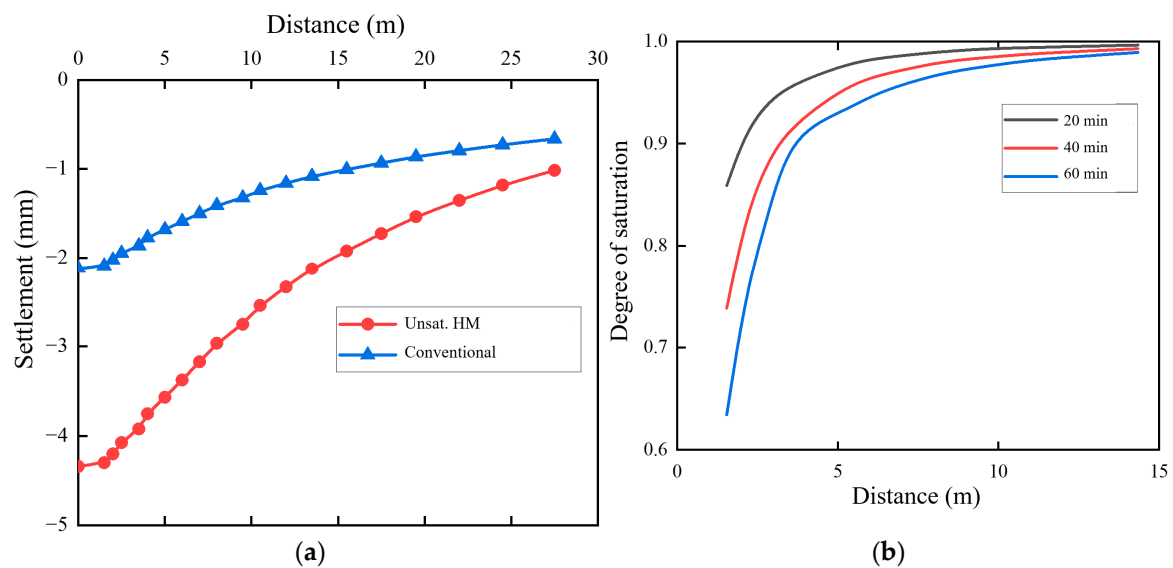


Figure 7. Comparison of simulation results between the conventional model and the unsaturated fluid–structure coupling model: (a) Ground settlement and deformation distribution map; (b) Degree of saturation distribution map at different time steps.

This chapter analyzed, across multiple comparison groups and pumping scenarios, the causes of differences in groundwater drawdown, ground settlement, and degree of saturation. From the drawdown perspective, the unsaturated fluid–structure coupling model better captures groundwater drawdown behavior in the later stage of pumping for granite residual soil, providing higher accuracy and closer agreement with field measurements than the conventional fluid–structure coupling model. From the settlement perspective, the unsaturated fluid–structure coupling model predicts more pronounced settlement responses. From the saturation perspective, the unsaturated fluid–structure coupling model enables direct visualization of the evolution of degree of saturation during engineering dewatering.

4. Factors Influencing Ground Settlement

Based on the three-dimensional numerical model for unsaturated fluid–structure coupling established in the previous section, an analysis of the factors influencing ground settlement was conducted. The impact of factors such as pumping rate and groundwater drawdown depth on the time and spatial distribution of soil settlement deformation was explored. This analysis aims to provide reference for engineering design, optimize construction strategies, reduce engineering risks, improve safety, and mitigate the adverse effects of soil settlement on the project and surrounding environment. Due to the unique nature of foundation pit projects, the requirements for different foundation pit constructions vary, which results in diverse dewatering schemes with different pumping rates and groundwater drawdown depths. Therefore, this study sets up several different scenarios to explore the settlement sensitivity of the soil during the engineering dewatering process.

4.1. Impact of Pumping Rate on Ground Settlement

Pumping rate refers to the speed at which water is extracted from the aquifer. The size of the pumping rate directly affects the effectiveness of dewatering and the settlement of surrounding areas. In engineering dewatering, the total drawdown depth is typically fixed,

while the pumping rate can be adjusted. Studying the effects of different pumping rates helps to clarify how pumping rate influences soil settlement and deformation.

(1) Scenario Setup

The pumping rate in the engineering dewatering process is represented by the discharge Q . To provide a more intuitive reflection of pumping rate, the pumping rate was converted into the rate of decrease in the water level at the dewatering well. With the total drawdown depth kept constant, three scenarios were set up, as shown in Table 4.

Table 4. Pumping rate scenarios.

Scenario	Drawdown Rate (m/min)	Total Pumping Time (min)	Total Drawdown (m)
Pumping Rate A	0.673	20	13.45
Pumping Rate B	0.336	40	13.45
Pumping Rate C	0.224	60	13.45

(2) Analysis of Calculation Results

The water level drawdown and distribution charts for each pumping rate scenario are shown in Figure 8a,b. It can be observed that as the pumping rate increases, the time for the dewatering well to reach the target drawdown decreases. However, when the pumping rate is higher, the drawdown in the soil farther from the well is smaller. This is due to the time required for soil permeability and the drainage process. The high pumping rate scenario leads to shorter dewatering times, resulting in a delay in the drainage process at greater distances, which is consistent with the studies Lewis [35], who found that soil water levels at distant locations exhibit a lag effect during pumping, where pore water pressure decreases and soil deformation follows the development over time.

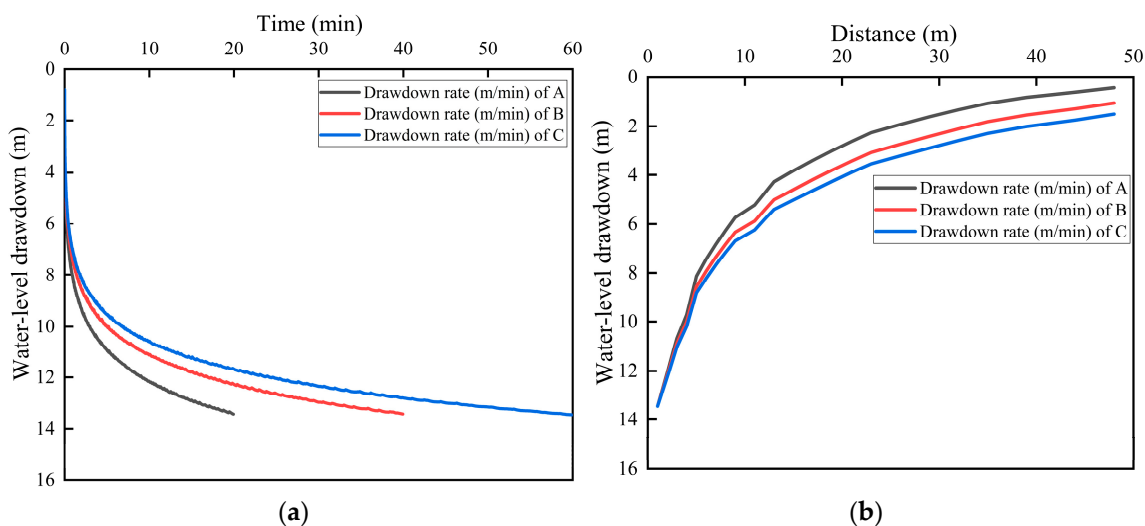


Figure 8. Groundwater Drawdown at Pumping Well for Different Pumping Rates: (a) Groundwater drawdown at the pumping well; (b) Drawdown depth distribution.

The soil settlement deformation distribution charts for each pumping rate scenario are shown in Figure 9a. The results indicate that as the pumping rate increases, the soil settlement deformation increases in the short term. However, when the target drawdown depth is reached, the scenario with the lowest pumping rate results in the largest total settlement deformation. This soil settlement deformation is composed of two parts: one caused by the reduction in pore water pressure, which increases effective stress and leads to immediate settlement, and another due to changes in porosity during drainage consoli-

dation, which accumulates over time. Pumping rate changes the pore-pressure dissipation rate and the recovery path of effective stress. This time effect can be described using a pore-pressure-based “degree of consolidation”. A slower drawdown generally corresponds to more sustained pore-pressure dissipation and effective-stress recovery, promoting greater volumetric strain accumulation, whereas a faster drawdown may cause rapid redistribution of pore pressure with relatively delayed volumetric strain accumulation. This description helps clarify the mechanisms underlying differences in settlement time histories under different pumping rates. In scenarios with lower pumping rates, the longer dewatering time results in more significant settlement caused by drainage consolidation. The distribution of soil settlement deformation for each pumping rate scenario is shown in Figure 9b. As shown, the settlement near the dewatering well is similar in all scenarios, and the difference in settlement due to drainage consolidation is relatively small. However, the settlement increases as the distance from the well increases, which is related to the lag effect of soil permeability. In scenarios with lower pumping rates, the soil pore water pressure is more fully released, resulting in larger settlement.

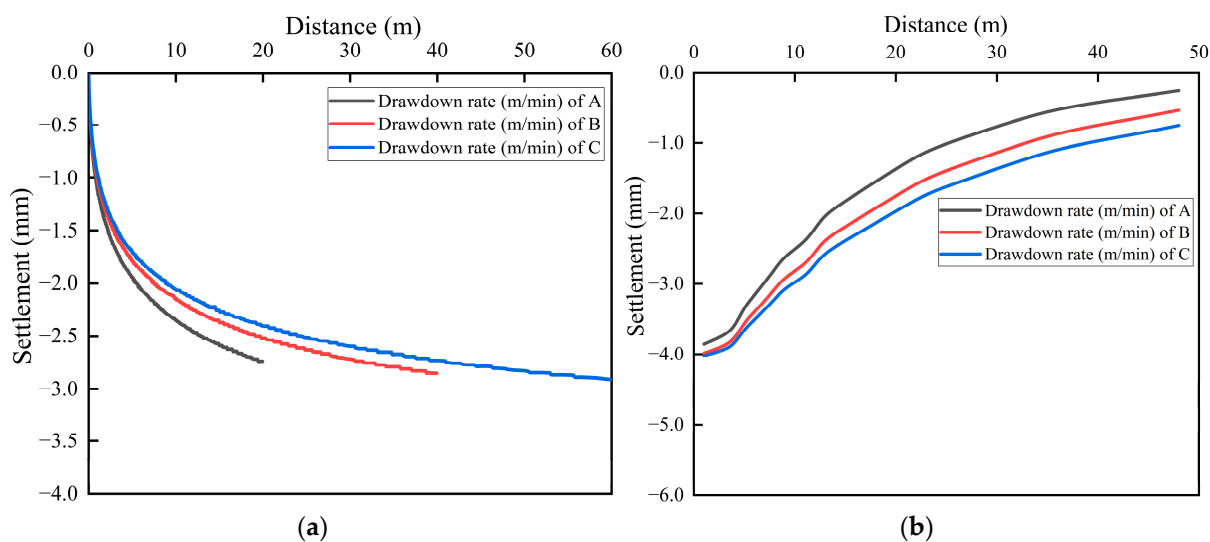


Figure 9. Soil Settlement at Pumping Well for Different Pumping Rates: (a) Settlement–time curve at the pumping well; (b) Ground settlement distribution map.

This calculation comprehensively explains the components of soil settlement deformation due to dewatering. Under the same target drawdown but different pumping rates, the minor differences in soil settlement near the dewatering well are mainly due to different drainage consolidation times, while the differences further from the dewatering well are primarily due to varying pore water pressure dissipation in the soil.

4.2. Impact of Groundwater Drawdown on Ground Settlement

(1) Scenario Setup

To study the effect of groundwater drawdown depth on soil settlement deformation, three scenarios were set up. One scenario was defined as the maximum drawdown depth, set as 100% of the target drawdown, while the other two scenarios were set to 75% and 50% of the target drawdown, respectively. The total pumping time was kept constant, as shown in Table 5.

(2) Analysis of Calculation Results

The water level drawdown charts for each groundwater drawdown depth scenario are shown in Figure 10a. It can be seen that, over the same time period, the curves for

all drawdown depth scenarios follow a similar trend, with approximately 80% of the target drawdown completed within the first ten minutes. The groundwater drawdown distribution for each scenario is shown in Figure 10b. Near the dewatering well, the drawdown depth matches the set scenario. However, as the distance from the dewatering well increases, the drawdown depth decreases, and the differences in drawdown depth among scenarios become smaller.

Table 5. Groundwater drawdown depth scenarios.

Scenario	Groundwater Drawdown (m)	Drawdown Percentage (%)	Total Pumping Time (min)
Drawdown Depth A	13.45	100	60
Drawdown Depth B	10.17	75	60
Drawdown Depth C	6.89	50	60

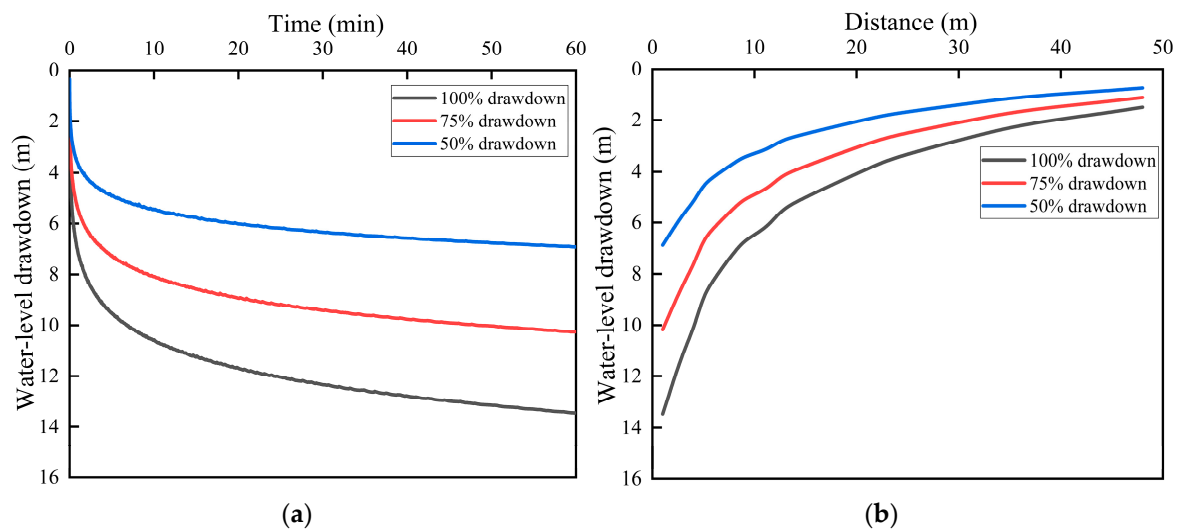


Figure 10. Groundwater Drawdown Depth Distribution Across Different Scenarios: (a) Groundwater drawdown at the pumping well; (b) Drawdown depth distribution.

The soil settlement deformation at the dewatering well for each groundwater drawdown depth scenario is shown in Figure 11a. It can be observed that with increasing dewatering time, the differences in soil settlement deformation among scenarios also increase. Figure 11b presents the soil settlement deformation distribution for each scenario, showing that the maximum deformation occurs near the dewatering well. The differences in settlement deformation are largest at the well and decrease with increasing distance, which follows the same trend as the groundwater drawdown distribution.

To further investigate the relationship between groundwater drawdown depth and soil settlement deformation over the same time period, a normalized analysis of the final settlement deformation and groundwater drawdown depth was conducted. The normalized relationship between water level drawdown and soil settlement deformation at the dewatering well is shown in Figure 12a. It can be seen that the soil settlement deformation at the dewatering well is proportional to the groundwater drawdown depth. The normalized analysis of drawdown depth and soil settlement deformation distribution is shown in Figure 12b. Using the 100% drawdown scenario as a reference, the settlement deformation for the 75% and 50% drawdown scenarios was normalized by dividing by the reference value. The results show that the lateral settlement deformation distribution is approximately proportional to the groundwater drawdown distribution. Therefore, for the same aquifer, the effect of groundwater drawdown depth on soil settlement deformation can be approximated as a linear relationship. The near-linear trend in the normalized drawdown–

settlement relationship is an empirical finding within the present ground conditions and dewatering durations. Its use should be limited to similar stratigraphy/parameters and comparable dewatering times; extrapolation to strongly heterogeneous or substantially different-duration cases should be treated with caution.

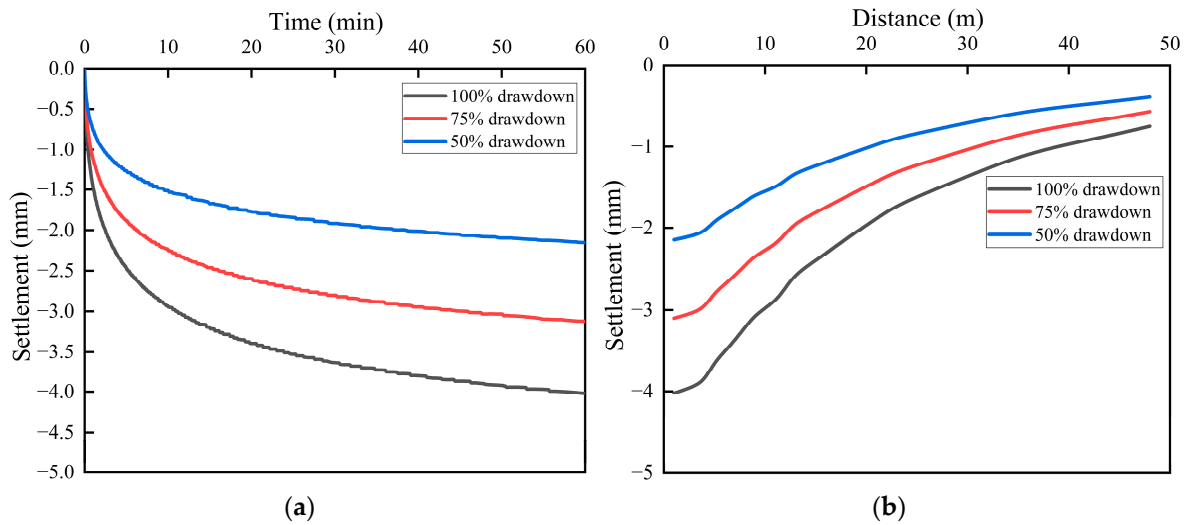


Figure 11. Soil Settlement Distribution Across Different Drawdown Depths: (a) Settlement–time curve at the pumping well; (b) Ground settlement distribution map.

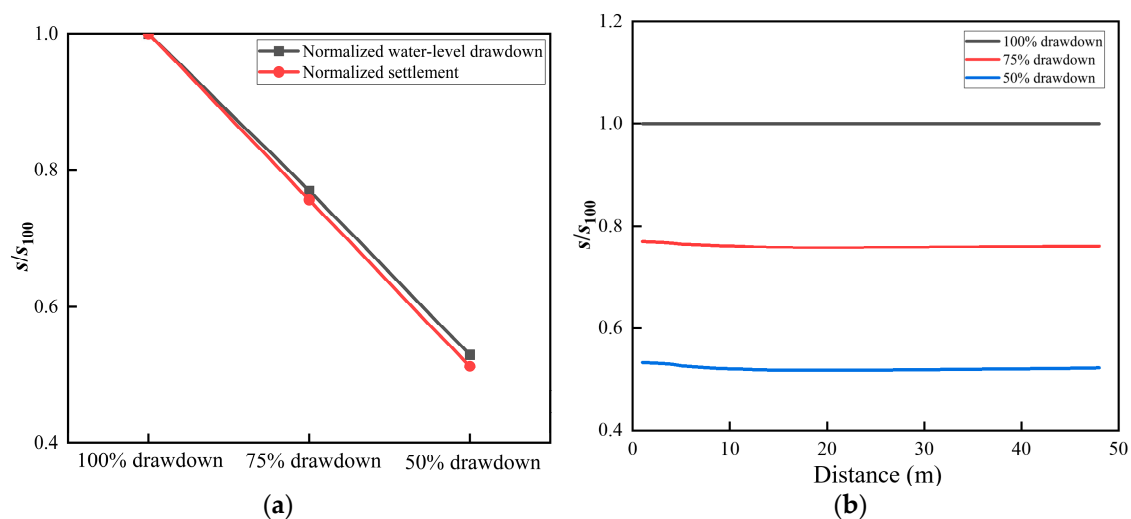


Figure 12. Normalized ground settlement deformation map: (a) Ground settlement at the pumping well; (b) Settlement deformation distribution.

5. Conclusions

This study uses numerical simulation methods and unsaturated fluid–structure coupling theory to investigate the settlement sensitivity of granite residual soil during foundation pit dewatering. The main conclusions are as follows:

- (1) For granite residual soil, the unsaturated fluid–structure coupling method provides better representation of settlement behavior compared to the traditional fluid–structure coupling model, especially with respect to groundwater drawdown. It also allows for the visualization of soil saturation during the dewatering process.
- (2) Under the same target drawdown depth but different pumping rates, the minor differences in soil settlement near the dewatering well are mainly due to variations in drainage consolidation time, whereas the differences in settlement further from the well are mainly attributed to the different pore water pressure dissipation rates.

- (3) The impact of groundwater drawdown depth on soil settlement deformation can be approximated as a near-linear relationship under the present ground conditions and within the range considered, for the same dewatering duration. Therefore, for large-scale dewatering, small-scale pre-tests with lower drawdown depths can be conducted, and the results can be scaled proportionally to predict the settlement deformation under the larger dewatering conditions, provided that the stratigraphy/parameters, initial saturation, and dewatering duration are comparable; extrapolation to substantially different conditions should be treated with caution.

Limitations: The settlement at this site is on the millimeter scale; its practical risk significance should therefore be judged in conjunction with monitoring accuracy, the sensitivity of adjacent structures, and allowable deformation criteria. The contribution of this study is to elucidate how unsaturated evolution affects late-stage drawdown and settlement time histories; its broader applicability depends on appropriate constraints on key hydraulic parameters (especially the SWCC and permeability functions) and consistency with site conditions. The three-dimensional numerical model in this study simplifies the actual structure of some soil layers, assuming the layer interfaces are planar and ignoring local variations in thickness. The heterogeneity and complexity of the actual strata may have different effects on the dewatering process and settlement deformation. Therefore, future work could consider a more refined stratification and the impact of soil heterogeneity on the model results. Additionally, the unsaturated soil parameters in this study were selected based on laboratory test results and literature data. However, due to the variability in soil properties in different regions, there may be some uncertainty in the model parameters. Future research could further calibrate and optimize the unsaturated soil parameters through multiple field tests to enhance the applicability and accuracy of the model. Although this study has conducted preliminary verification through field pumping tests and numerical simulations, the verification process is still incomplete due to the limited field test data and monitoring scope. Accordingly, the main conclusions regarding the improved representation of unsaturated effects are supported by the validated drawdown response, whereas settlement-related findings should be interpreted as model-based predictions pending further field monitoring. Future work could further validate and optimize the model's performance by collecting more extensive field data, setting up more operating conditions, and comparing results from different models.

Author Contributions: Conceptualization, Z.L.; Methodology, Z.L., S.N. and Z.P.; Formal analysis, Z.L., S.N. and Z.P.; Investigation, Z.L., S.N. and Z.P.; Data curation, Z.L., S.N. and Z.P.; Writing—original draft, Z.L., S.N. and Z.P.; Writing—review & editing, Y.S.; Visualization, Z.L., S.N. and Z.P.; Supervision, Y.L. and Y.S.; Project administration, Y.L.; Funding acquisition, Y.L., J.C. and Y.S. All authors have read and agreed to the published version of the manuscript.

Funding: This research was funded by the Guangzhou Science and Technology Research Program for Graduate Students in Higher Education Institutions (Grant Number. 2024312342).

Data Availability Statement: The original contributions presented in the study are included in the article; further inquiries can be directed to the corresponding author.

Conflicts of Interest: The authors declare that the research was conducted in the absence of any commercial or financial relationships that could be construed as a potential conflict of interest.

References

1. Li, K.; Chen, S.; Pei, R.; Chen, J. Theoretical Prediction Study on Drawdown and Surface Settlement Induced by Dewatering and Excavation in Unconfined Aquifers. *Comput. Geotech.* **2025**, *179*, 107041. [[CrossRef](#)]
2. Xie, Z.-F.; Shen, S.-L.; Arulrajah, A.; Horpibulsuk, S. Environmentally Sustainable Groundwater Control during Dewatering with Barriers: A Case Study in Shanghai. *Undergr. Space* **2021**, *6*, 12–23. [[CrossRef](#)]

3. Wu, Y.-X.; Lyu, H.-M.; Han, J.; Shen, S.-L. Dewatering-Induced Building Settlement around a Deep Excavation in Soft Deposit in Tianjin, China. *J. Geotech. Geoenviron. Eng.* **2019**, *145*, 05019003. [[CrossRef](#)]
4. Zeng, C.-F.; Wang, S.; Xue, X.-L.; Zheng, G.; Mei, G.-X. Characteristics of Ground Settlement Due to Combined Actions of Groundwater Drawdown and Enclosure Wall Movement. *Acta Geotech.* **2022**, *17*, 4095–4112. [[CrossRef](#)]
5. Zhang, X.; Yang, J.; Zhang, Y.; Gao, Y. Cause Investigation of Damages in Existing Building Adjacent to Foundation Pit in Construction. *Eng. Fail. Anal.* **2018**, *83*, 117–124. [[CrossRef](#)]
6. Wen, D.; Lin, K.Q. The Effect of Deep Excavation on Pore Water Pressure Changes in the Old Alluvium and Under-Drainage of Marine Clay in Singapore. In *Geotechnical Aspects of Underground Construction in Soft Ground*; Spécifique: Lyon, France, 2002.
7. Jia, R.; Shan, Y.; Yang, K.; Wang, Y.; Hu, Z.; Li, Y.; Cui, J. Effect of Suffosion on Deterioration of Weathered Granite Soil: A Multi-Scale Study from Macroscopic to Microscopic Investigations. *Acta Geotech.* **2025**, *20*, 4213–4229. [[CrossRef](#)]
8. Shan, Y.; Yang, K.; Jia, R.; Li, Y.; Wang, Y.; Cui, J. Mechanical Behavior and Compositional Variation of Weathered Granite Soil with Different Degrees of Weathering. *Bull. Eng. Geol. Environ.* **2025**, *84*, 39. [[CrossRef](#)]
9. Li, Q.; Zheng, G.; Cheng, X.; Shi, X.; Zhang, N.; Zhou, S.; Cheng, W. Deformation and Protection of Tunnels Influenced by Excavation Dewatering in Soft Soil Strata with Leaky Aquifers. *Tunn. Undergr. Space Technol.* **2025**, *159*, 106468. [[CrossRef](#)]
10. Li, M.-G.; Chen, J.-J.; Xia, X.-H.; Zhang, Y.-Q.; Wang, D.-F. Statistical and Hydro-Mechanical Coupling Analyses on Groundwater Drawdown and Soil Deformation Caused by Dewatering in a Multi-Aquifer-Aquitard System. *J. Hydrol.* **2020**, *589*, 125365. [[CrossRef](#)]
11. Wang, S.; Wang, W.; Xu, Z.; Song, Q.; Qian, J. Field Pumping and Recharge Test Study for Confined Aquifers in Super-Large Deep Foundation Pit Group Sites. *Buildings* **2025**, *15*, 1383. [[CrossRef](#)]
12. Thomas, H.R.; Rees, S.W. The Numerical Simulation of Seasonal Soil Drying in an Unsaturated Clay Soil. *Int. J. Numer. Anal. Methods Géoméch.* **1993**, *17*, 119–132. [[CrossRef](#)]
13. Chu, Y.; Shi, J.; Ye, Z.; Liu, D. Dewatering Characteristics and Drawdown Prediction of Suspended Waterproof Curtain Foundation Pit in Soft Soil Areas. *Buildings* **2024**, *14*, 119. [[CrossRef](#)]
14. Yin, S.; Liu, P.; Kong, L.; Zhang, X.; Qi, Y.; Huang, J. Accumulated Plastic Strain Behavior of Granite Residual Soil under Traffic Loading. *Soil Dyn. Earthq. Eng.* **2023**, *164*, 107617. [[CrossRef](#)]
15. Zhu, Y.; Wang, W.; Xu, Z.; Chen, J.; Zhang, J. Hydro-Mechanical Numerical Analysis of a Double-Wall Deep Excavation in a Multi-Aquifer Strata Considering Soil-Structure Interaction. *Buildings* **2025**, *15*, 989. [[CrossRef](#)]
16. Pujades, E.; Vázquez-Suñé, E.; Carrera, J.; Vilarrasa, V.; De Simone, S.; Jurado, A.; Ledesma, A.; Ramos, G.; Lloret, A. Deep Enclosures versus Pumping to Reduce Settlements during Shaft Excavations. *Eng. Geol.* **2014**, *169*, 100–111. [[CrossRef](#)]
17. Zhang, Y.-Q.; Li, M.-G.; Wang, J.-H.; Chen, J.-J.; Zhu, Y.-F. Field Tests of Pumping-Recharge Technology for Deep Confined Aquifers and Its Application to a Deep Excavation. *Eng. Geol.* **2017**, *228*, 249–259. [[CrossRef](#)]
18. Sun, Y.; Jiang, Z.; Tong, L.; Sun, J.; Cui, J.; Zhou, X.; Liu, S. Optimization of Confined Aquifer Dewatering for Long-Deep Excavation Using Simulation-Optimization Method. *Undergr. Space* **2024**, *17*, 246–266. [[CrossRef](#)]
19. Cai, G.; Han, B.; Li, M.; Di, K.; Liu, Y.; Li, J.; Wu, T. Numerical Implementation of a Hydro-Mechanical Coupling Constitutive Model for Unsaturated Soil Considering the Effect of Micro-Pore Structure. *Appl. Sci.* **2021**, *11*, 5368. [[CrossRef](#)]
20. Wang, L.; Shen, C.; Liu, S.; Alonso, E.; Huang, P. A Hydro-Mechanical Coupled Solution for Electro-Osmotic Consolidation in Unsaturated Soils Considering the Decrease in Effective Voltage with Time. *Comput. Geotech.* **2021**, *133*, 104050. [[CrossRef](#)]
21. Zhang, W.; Ran, B.; Gu, X.; Zhang, Y.; Zou, Y.; Wang, P. Efficient Reliability Analysis of Unsaturated Slope Stability under Rapid Drawdown Using XGBoost-Based Surrogate Model. *Soils Found.* **2024**, *64*, 101539. [[CrossRef](#)]
22. Fung, W.T. Experimental Study and Centrifuge Modeling of Loose Fill Slope. Ph.D. Thesis, Hong Kong University of Science and Technology, Hong Kong, China, 2001.
23. Fredlund, D.G.; Xing, A. Equations for the Soil-Water Characteristic Curve. *Can. Geotech. J.* **1994**, *31*, 521–532. [[CrossRef](#)]
24. Ou, C.-Y.; Chiou, D.-C.; Wu, T.-S. Three-Dimensional Finite Element Analysis of Deep Excavations. *J. Geotech. Engrg.* **1996**, *122*, 337–345. [[CrossRef](#)]
25. Ou, C.-Y.; Shiau, B.-Y.; Wang, I.-W. Three-Dimensional Deformation Behavior of the Taipei National Enterprise Center (TNEC) Excavation Case History. *Can. Geotech. J.* **2000**, *37*, 438–448. [[CrossRef](#)]
26. Hsiung, B.-C.B.; Yang, K.-H.; Aila, W.; Hung, C. Three-Dimensional Effects of a Deep Excavation on Wall Deflections in Loose to Medium Dense Sands. *Comput. Geotech.* **2016**, *80*, 138–151. [[CrossRef](#)]
27. Wu, Y.-X.; Shen, S.-L.; Lyu, H.-M.; Zhou, A. Analyses of Leakage Effect of Waterproof Curtain during Excavation Dewatering. *J. Hydrol.* **2020**, *583*, 124582. [[CrossRef](#)]
28. Zeng, C.-F.; Powrie, W.; Chen, H.-B.; Wang, S.; Diao, Y.; Xue, X.-L. Ground Behavior Due to Dewatering Inside a Foundation Pit Considering the Barrier Effect of Preexisting Building Piles on Aquifer Flow. *J. Geotech. Geoenviron. Eng.* **2024**, *150*, 05024004. [[CrossRef](#)]
29. Van Genuchten, M.T. A Closed-form Equation for Predicting the Hydraulic Conductivity of Unsaturated Soils. *Soil Sci. Soc. Am. J.* **1980**, *44*, 892–898. [[CrossRef](#)]

30. Mualem, Y. A New Model for Predicting the Hydraulic Conductivity of Unsaturated Porous Media. *Water Resour. Res.* **1976**, *12*, 513–522. [[CrossRef](#)]
31. Bresciani, E.; Shandilya, R.N.; Kang, P.K.; Lee, S. Well Radius of Influence and Radius of Investigation: What Exactly Are They and How to Estimate Them? *J. Hydrol.* **2020**, *583*, 124646. [[CrossRef](#)]
32. Ren, G.; Buckeridge, J.; Li, J. Estimating Land Subsidence Induced by Groundwater Extraction in Unconfined Aquifers Using an Influence Function Method. *J. Water Resour. Plan. Manag.* **2015**, *141*, 04014084. [[CrossRef](#)]
33. Rudolph, D.L.; Sudicky, E.A. Simulation of Groundwater Flow in Complex Multiaquifer Systems: Performance of a Quasi Three-Dimensional Technique in the Steady-State Case. *Can. Geotech. J.* **1990**, *27*, 590–600. [[CrossRef](#)]
34. Shen, Q.; Zhou, Z.; Li, Y. Three-Dimensional Nonlinear Flow Numerical Simulation Considering the Distribution of Interlayer Shear Weakness Zones: A Case Study in Baihetan Hydropower Project, China. *Bull. Eng. Geol. Environ.* **2022**, *81*, 15. [[CrossRef](#)]
35. Lewis, R.W.; Schrefler, B. A Fully Coupled Consolidation Model of the Subsidence of Venice. *Water Resour. Res.* **1978**, *14*, 223–230. [[CrossRef](#)]

Disclaimer/Publisher’s Note: The statements, opinions and data contained in all publications are solely those of the individual author(s) and contributor(s) and not of MDPI and/or the editor(s). MDPI and/or the editor(s) disclaim responsibility for any injury to people or property resulting from any ideas, methods, instructions or products referred to in the content.